# Nicotinamide mononucleotide synthetase is the key enzyme for an alternative route of NAD biosynthesis in *Francisella tularensis*

**Leonardo Sorci[a], Dariusz Martynowski[b], Dmitry A. Rodionov[a,c], Yvonne Eyobo[b], Xhavit Zogaj[d], Karl E. Klose[d], Evgeni V. Nikolaev[e], Giulio Magni[f], Hong Zhang[b], and Andrei L. Osterman[a,g,1]**

[a]Burnham Institute for Medical Research, 10901 North Torrey Pines Road, La Jolla, CA 92037; [b]Department of Biochemistry, University of Texas Southwestern Medical Center, Dallas, TX 75390; [d]South Texas Center for Emerging Infectious Diseases, University of Texas, San Antonio, TX 78249; [e]Department of Pathology, Anatomy and Cell Biology, and Daniel Baugh Institute for Functional Genomics and Computational Biology, Thomas Jefferson University, Philadelphia, PA 19107; [f]Istituto di Biotecnologie Biochimiche, Università Politecnica delle Marche, 60131 Ancona, Italy; [g]Fellowship for Interpretation of Genomes, Burr Ridge, IL 60527; and [c]Institute for Information Transmission Problems, 127994 Moscow, Russia

Edited by Gregory A. Petsko, Brandeis University, Waltham, MA, and approved December 30, 2008 (received for review November 19, 2008)

**Enzymes involved in the last 2 steps of nicotinamide adenine dinucleotide (NAD) cofactor biosynthesis, which catalyze the adenylylation of the nicotinic acid mononucleotide (NaMN) precursor to nicotinic acid dinucleotide (NaAD) followed by its amidation to NAD, constitute promising drug targets for the development of new antibiotics. These enzymes, NaMN adenylyltransferase (gene *nadD*) and NAD synthetase (gene *nadE*), respectively, are indispensable and conserved in nearly all bacterial pathogens. However, a comparative genome analysis of *Francisella tularensis* allowed us to predict the existence of an alternative route of NAD synthesis in this category A priority pathogen, the causative agent of tularaemia. In this route, the amidation of NaMN to nicotinamide mononucleotide (NMN) occurs before the adenylylation reaction, which converts this alternative intermediate to the NAD cofactor. The first step is catalyzed by NMN synthetase, which was identified and characterized in this study. A crystal structure of this enzyme, a divergent member of the NadE family, was solved at 1.9-Å resolution in complex with reaction products, providing a rationale for its unusual substrate preference for NaMN over NaAD. The second step is performed by NMN adenylyltransferase of the NadM family. Here, we report validation of the predicted route (NaMN → NMN → NAD) in *F. tularensis* including mathematical modeling, in vitro reconstitution, and in vivo metabolite analysis in comparison with a canonical route (NaMN → NaAD → NAD) of NAD biosynthesis as represented by another deadly bacterial pathogen, *Bacillus anthracis*.**

genomic reconstruction | in vitro reconstitution | mathematical modeling | NAD intermediates | substrate preference

Biosynthesis of NAD, an indispensable and universal redox cofactor, has been the subject of extensive studies in a variety of species (1–3). Despite some variations in the early steps of the de novo and salvage pathways, the final biochemical transformations from the committed NaMN intermediate to NAD appear to be the same across all 3 domains of life. The 2 consecutive steps, referred to here as conventional route I, include the adenylylation of NaMN to NaAD followed by the ATP-dependent amidation of NaAD to NAD (Fig. 1). In bacteria, the first step is catalyzed by the enzyme NaMN adenylyltransferase of the NadD family. Genes encoding both enzymes are conserved and are essential in most pathogenic bacteria, and thus constitute prominent targets for the development of new antibiotics (4–8). The nearly universal character of biosynthetic route I is supported by the observed strict cooccurrence of *nadD* and *nadE* genes in the overwhelming majority of bacterial species with completely sequenced genomes [>750 genomes in the current version of NAD(P) biosynthesis subsystem in The SEED (9), also see *SI Appendix*, Table S1]. Route I is shared by both de novo synthesis from L-aspartate (genes *nadB-nadA-nadC*) and nicotinic acid salvage (genes *pncA-pncB*) pathways that converge at the common NaMN intermediate. Most bacteria have both pathways, as illustrated here for *Bacillus anthracis* (Fig. 1 and *SI Appendix*, Fig. S2), whereas some are strictly dependent on either de novo (e.g., *Helicobacter pylori*) or salvage (e.g., *Streptococcus pneumoniae*) pathways. The rarely observed absence of either

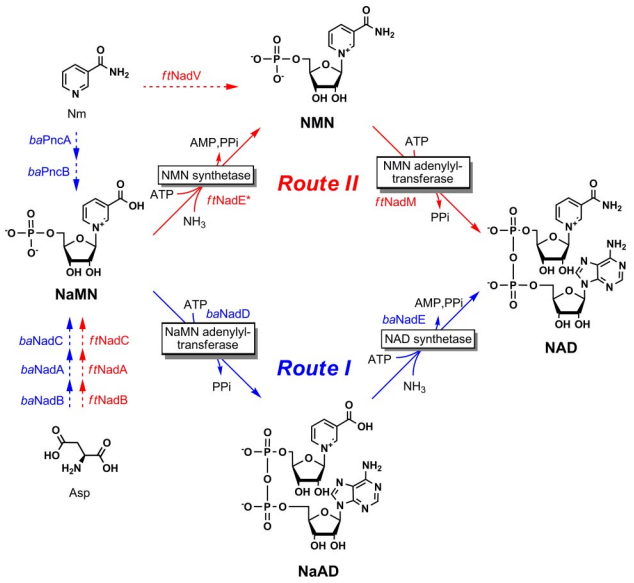


**Fig. 1.** Genomic reconstruction of NAD biosynthesis in *F. tularensis* and *B. anthracis*. In conventional route I, as occurs in *B. anthracis* (outlined in blue), NaMN is adenylated to NaAD by *ba*NadD, which is then amidated to NAD by NAD synthetase *ba*NadE. In route II postulated for *F. tularensis* (outlined in red), an NMN synthetase activity of *ft*NadE* amidates the NaMN precursor to NMN before its adenylylation by *ft*NadM. De novo biosynthesis of NaMN from aspartate (via NadB, NadA, and NadC enzymes), a common route for both species, and 2 alternative Nm salvage pathways, deamidating (via PncA and PncB enzymes as in *B. anthracis*) and nondeamidating (via NadV enzymes as in *F. tularensis*), are shown by dashed arrows with respective color coding.

Author contributions: L.S. and A.L.O. designed research; L.S., D.M., Y.E., X.Z., and E.V.N. performed research; L.S. contributed new reagents/analytic tools; L.S., D.A.R., K.E.K., G.M., H.Z., and A.L.O. analyzed data; and L.S., H.Z., and A.L.O. wrote the paper.

The authors declare no conflict of interest.

This article is a PNAS Direct Submission.

Data deposition: The coordinates and structure factors for the *ft*NadE* complex with AMP, PPi, and metal ions have been deposited in the Protein Data Bank, www.pdb.org (PDB ID code 3FIU).

[1]To whom correspondence should be addressed. E-mail: osterman@burnham.org.

This article contains supporting information online at www.pnas.org/cgi/content/full/0811718106/DCSupplemental.

pathway strongly correlates with the absence of both *nadD* and *nadE* genes. For example, *Haemophilus influenzae* overcomes this deficiency by the salvage of nicotinamide riboside (RNm) via NMN adenylyltransferase of the NadR family (10). In some intracellular pathogens with truncated genomes (such as *Chlamydia* spp), the loss of the entire NAD biosynthetic machinery is compensated for by the uptake of the intact cofactor from the host cells (11). A comparative genomic reconstruction of NAD biosynthesis within the collection of completely sequenced bacterial genomes integrated in The SEED allowed us to hypothesise that, in contrast to all previously studied species, the final 2 steps of NAD biosynthesis in *Francisella tularensis* occur in reverse order. In this pathogen, the amidation of NaMN to NMN appears to precede the adenylylation step converting NMN to NAD (Fig. 1). The enzymes involved in this pathway (here termed route II) were identified and characterized. The first reaction of route II is catalyzed by a divergent member of the NadE family endowed with NMN synthetase activity. Steady-state kinetic characteristics of this newly identified enzyme (here denoted *ft*NadE* to emphasize its distinction from other members of the NadE family with NAD synthetase activity) were established. The 3D structure of *ft*NadE* in complex with reaction products was solved at 1.9-Å resolution, revealing active site features that are likely responsible for its strong preference for NaMN vs. NaAD substrate. The in vivo NMN synthetase function of *ft*NadE* was verified by activity and metabolite measurements in crude extracts of the wild-type and Δ*nadE** mutant of *F. tularensis* subsp *novicida.* The second step of route II is catalyzed by the NMN-preferring adenylyltransferase of the NadM family. This activity is encoded within the N-terminal domain of the *ft*NadM/Nudix bifunctional protein whose 3D structure and some enzymatic properties were reported in ref. 5. Here, we used a mixture of the purified recombinant enzymes *ft*NadE* and *ft*NadM for the experimental validation of the predicted pathway by its in vitro reconstitution with HPLC-based monitoring of the reaction products and intermediates. Similar experiments were performed using purified recombinant enzymes *ba*NadD and *ba*NadE from *B. anthracis*, representing a typical route I of NAD synthesis. The obtained results were consistent with a generalized mathematical model of the 2-step conversion of NaMN to NAD. In addition to establishing a precedent of this unexplored NAD biosynthetic route, this study provides new guidelines for targeting NAD biosynthesis in *F. tularensis*.

## Results

**Genomic Reconstruction and Prediction of the Alternative Route of NAD Biosynthesis in *F. tularensis*.** We used a subsystems-based approach implemented in The SEED (9) for the genomic reconstruction and analysis of variations in NAD biosynthesis across the entire collection of completely sequenced bacterial genomes. The results of this analysis are available online in the respective subsystem ("NAD and NADP cofactor biosynthesis global" at www.nmpdr.org (12)) and are shown in the condensed form in *SI Appendix*, Table S1. Among other features, this analysis confirmed the nearly universal cooccurrence of NaMN adenylyltransferase (gene *nadD*) and NAD synthetase (gene *nadE*) that jointly comprise a classic 2-step conversion of NaMN to NAD via the NaAD intermediate (route I in Fig. 1). Moreover, the NadD enzyme is present in *all* bacterial pathogens that contain genes of NaMN de novo synthesis from L-aspartate (*nadB*, *nadA*, and *nadC*), with the singular exception of *F. tularensis.*

The presence of NAD de novo synthesis in *F. tularensis* inferred by genomic reconstruction (operon *nadACB*) is consistent with the known ability of this pathogen to grow on defined media in the absence of nicotinamide or any other NAD precursors (13). However, the *nadD* gene, which is required for the utilization of the produced NaMN by conventional route I, is missing in all 7 available genomes of *F. tularensis* strains and isolates (*SI Appendix*, Table S2 and Fig. S2). In this context, the presence of the *nadE* gene in *F. tularensis* genomes appears equally unusual, because its anticipated NAD synthetase activity would be obsolete without a supply of NaAD substrate, which is typically produced by the NadD enzyme. The absence of 1 of the 2 recognized drug targets (NadD) and an unclear physiological context of the second target (NadE) in *F. tularensis*, a high-priority pathogen, prompted us to further analyze this conundrum.

**Table 1. Comparison of kinetic parameters of the enzymes involved in the last two steps of NAD synthesis in *F. tularensis* and *B. anthracis***

| Protein, substrate | Kinetic constants | | $k_{cat}/K_m$, $s^{-1}\cdot M^{-1}$ | Subs. pref., fold |
|---|---|---|---|---|
| | $k_{cat}$, $s^{-1}$ | $K_m$, mM | | |
| Amidation step | | | | |
| *ft*NadE*, NaMN | 0.50 ± 0.02 | 0.20 ± 0.04 | 2,500 | ≈60[†] |
| *ft*NadE*, NaAD | 0.25 ± 0.02 | 5.82 ± 1.13 | 43 | |
| *ba*NadE, NaMN | 0.004 ± 0.0002 | 1.18 ± 0.17 | 3 | ≈3,000[‡] |
| *ba*NadE, NaAD | 2.64 ± 0.06 | 0.29 ± 0.02 | 9,100 | |
| Adenylylation step | | | | |
| *ft*NadM, NaMN | 0.16 ± 0.01 | 0.81 ± 0.27 | 200 | ≈400[§] |
| *ft*NadM, NMN | 2.8 ± 0.1 | 0.034 ± 0.004 | 82,000 | |
| *ba*NadD, NaMN | 25.60 ± 1.2 | 0.04 ± 0.01 | 640,000 | ≈45,000[¶] |
| *ba*NadD, NMN | 0.014 ± 0.001 | 0.94 ± 0.12 | 15 | |

The apparent values of $K_m$ (mM) and $k_{cat}$ ($s^{-1}$) of *ft*NadE* and *ba*NadE enzymes for amidation of both alternative substrates, NaMN and NaAD, at saturating concentrations of ATP (2 mM) and $NH_4Cl$ (4 mM), and of *ba*NadD and *ft*NadM enzymes for adenylylation of NaMN and NMN at saturating concentration of ATP (2 mM) were determined as described in *SI Appendix*, SI Text. Errors represent standard deviation. Substrate preference (Subs. pref.) is expressed as a ratio of catalytic efficiencies ($k_{cat}^{app}/K_m^{app}$) for the respective alternative substrates (see *SI Appendix*, SI Fig. 5 for kinetic rate plots).
[†]NaMN > NaAD; [‡]NaAD > NaMN; [§]NMN > NaMN; [¶]NaMN > NMN.

The presence of orthologs of *nadV* and *nadM* genes encoding nicotinamide phosphoribosyl transferase and NMN adenylyltransferase in the *F. tularensis* genome pointed to a possible nicotinamide (Nm) salvage/recycling pathway (Fig. 1). The existence of such a 2-step conversion (Nm → NMN → NAD) was described in some bacteria (14, 15) and mammals (16). Although the presence of this salvage pathway in *F. tularensis* was further confirmed in our study (see below), this finding alone could not explain the growth of *F. tularensis* in the absence of Nm, nor could it suggest a physiological role for the nadE gene. A dual role of the *ft*NadM enzyme as both NMN and NaMN adenylyltransferase could be considered among possible interpretations of the gapped de novo pathway. Indeed, a single enzyme with comparable activity toward both NaMN and NMN intermediates is involved in NAD synthesis in mammalian cells (17–19). However, a strong preference of *ft*NadM for NMN over NaMN substrate (≈400-fold based on the comparison of respective $k_{cal}/K_m$ values, see Table 1) made this enzyme an unlikely candidate for the role of a missing NaMN adenylyltransferase in conventional route I (NaMN → NaAD → NAD) (5).

Among other interpretations, the most compelling (albeit unconventional) was the hypothesis of the alternative pathway from NaMN to NAD with the opposite order of amidation and adenylylation steps (NaMN → NMN → NAD). This pathway (route II in Fig. 1) would proceed via the NMN (as opposed to the NaAD) intermediate, allowing the *ft*NadM enzyme to efficiently catalyze the NMN adenylyltransferase reaction at the second step of the pathway. An enzymatic activity inferred for the first step of the proposed pathway was termed NMN synthetase by analogy with the NAD synthetase reaction of NadE enzymes. Indeed, the postulated enzyme would catalyze essentially the same chemical transformation (ATP-dependent amidation of pyridine carboxylate) with the only feature differentiating NaMN and NAD substrates, the absence of an adenylyl moiety, being remote from the

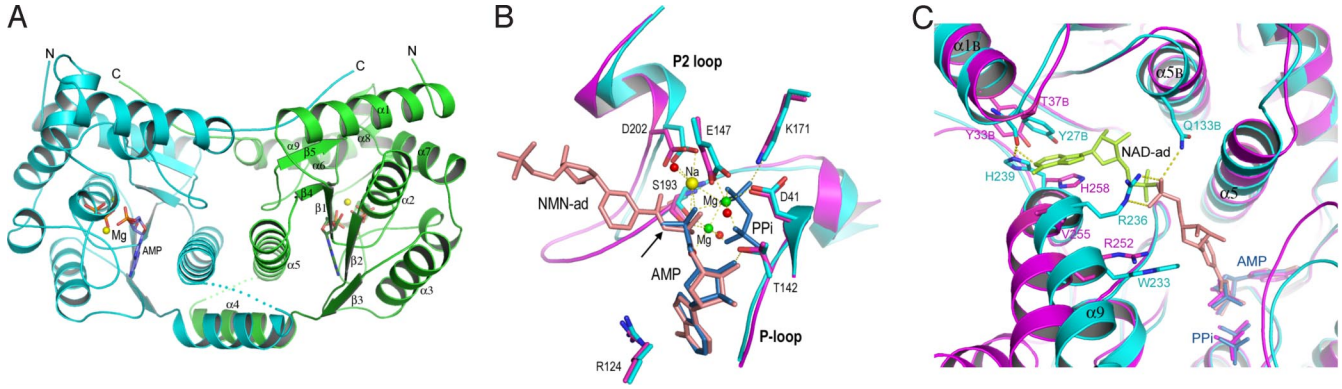


**Fig. 2.** Three-dimentional structure of NMN synthetase from *F. tularensis* (*ft*NadE*) and a comparison with *B. anthracis* NAD synthetase (*ba*NadE) structure. (*A*) Overall structure of *ft*NadE* (cyan and green subunits) homodimer is shown with bound AMP, PPi, and catalytic metal ions. (*B* and *C*) Superposition of *ft*NadE* (cyan) and *ba*NadE (magenta) is illustrated by a detailed view of the catalytic sites (*B*) and substrate binding pockets (*C*). The arrow points to the nicotinosyl carboxyl group that is adenylated in the *ba*NadE complex and that would be amidated in the second step of the reaction.

actual site of the reaction. Hence, it was tempting to suggest the product of the *F. tularensis nadE* gene a candidate for the proposed functional role of NMN synthetase (termed *ft*NadE*). Despite the straightforward chemical analogy, this alternative activity was previously never detected (20, 21), and, in most cases, this activity was not assayed for any of the characterized members of the NadE family (22–28). To test the bioinformatic predictions described above, we performed the kinetic and structural characterization of purified recombinant *ft*NadE* enzyme.

**Enzymatic Characterization of *ft*NadE* Endowed with NMN Synthetase Activity.** The gene (FTL0685) encoding for *ft*NadE* from *F. tularensis* subsp. *novicida* strain U112 was cloned and overexpressed in *E. coli* with the N-terminal 6xHis tag. The recombinant *ft*NadE* protein was purified to homogeneity (*SI Appendix*, Fig. S3), using Ni-affinity chromatography, followed by gel filtration. The predicted NMN synthetase activity of *ft*NadE* was initially confirmed by a developed colorimetric coupled assay. It was then directly verified, kinetically characterized, and compared with a relatively low NAD synthetase activity also displayed by *ft*NadE*, using the HPLC-based protocol (*SI Appendix*, Fig. S4). The reaction requires conversion of 1 molecule of ATP to AMP and $PP_i$ per cycle of amidation of NaMN to NMN (as confirmed by HPLC, *SI Appendix*, Fig. S9). This is consistent with the known catalytic mechanism of all members of the ATP-dependent amidotransferase superfamily (29), including NAD synthetases of the NadE family (30). We have also demonstrated that *ft*NadE* can use only ammonia ($NH_3$) but not glutamine (Gln) for the amidation of its substrate, consistently with the known properties of many bacterial NadE enzymes that do not contain an additional Gln-utilization (GAT) domain (22). The steady-state kinetic parameters of the *ft*NadE* enzyme shown in Table 1 revealed the enzyme's strong preference for the NaMN vs. the NaAD substrate. The conversion of NaMN to NMN with ATP and $NH_3$ as cosubstrates is catalyzed by *ft*NadE* with ≈60-fold higher efficiency than the amidation of the canonical NaAD substrate, based on the ratio of the respective $k_{cat}/K_m$ values. In contrast, we observed a >1,000-fold preference of NAD synthetase over NMN synthetase activity at saturating concentrations of each substrate for 2 other tested representatives of the NadE family from *Corynebacterium glutamicum* and *Helicobacter pylori* (*SI Appendix*, Table S3). Similar observations were made for the *ba*NadE enzyme that was studied here in more detail (see below). All observed substrate preferences were fully consistent with the different physiological roles of *ft*NadE* in route II vs. NadE involved in conventional route I of NAD biosynthesis in other species, based on genomic reconstruction (*SI Appendix*, Table S1). Although some of these and other members of the NadE family were structurally and mechanistically characterized, the structural basis of their NaAD vs. NMN substrate preference was never addressed before, because the existence of the NMN synthetase activity in this family was previously unknown. To address this question, we used the comparative structural analysis as described below.

**Structural Analysis of *ft*NadE* and Its Mechanistic Implications.** We crystallized and solved the 3-dimensional structure of *ft*NadE* complexed with the products of ATP hydrolysis, AMP and pyrophosphate (PPi), and Mg ions at 1.9-Å resolution (Fig. 2*A* and *SI Appendix*, Fig. S6). A comparison with a recently published 3D structure of *ba*NadE (1.28-Å average $C_\alpha$ RMSD) reveals a similar dimer organization (Fig. 2*A*), in which each subunit contributes to a partially shared active site (28). Most of the active site residues that provide key interactions with ATP, Mg ions, and ammonia (as originally mapped in the most detailed structure-function analysis of *bs*NadE (31)) are conserved in *ft*NadE*. Modeling of the NaMN substrate in the active site of *ft*NadE* suggests that it is likely to occupy the same position as the nicotinosyl moiety of NaAD in *ba*NadE complex (Fig. 2*B*). The structural conservation within the catalytic site suggests that NMN synthetase shares key mechanistic aspects with other NAD synthetases, including activation of the pyridine carboxyl-group by transient adenylylation and further displacement of the AMP-moiety by ammonia leading to the formation of a carboxamido-group (30). This is in agreement with the stoichiometric ATP-to-AMP conversion observed in the course of the *ft*NadE*-driven NMN synthetase reaction (as described above).

A detailed comparison of *ft*NadE* and *ba*NadE substrate binding pockets revealed structural differences that are likely to be responsible for the distinct substrate preferences of these enzymes. In the putative nicotinosyl binding site of *ft*NadE*, a replacement of *ba*NadE residues Gly-149 and Arg-252 by Gln and Trp, respectively, together with the significant movements in the α9 helix (≈3.5 Å) and the α5 helix (≈1.0 Å) generate a tighter substrate binding pocket that would be more favorable for the binding of the mononucleotide substrate. A replacement of *ba*NadE residue Val-255 by Arg in *ft*NadE* would provide additional interactions with a free phosphoryl group of NaMN (Fig. 2*C*). In the putative adenosyl binding site, a bulky side-chain of Tyr replacing *ba*NadE Thr-37 in the *ft*NadE* structure would block the adenosyl moiety of NaAD (Fig. 2*C*). Additionally, a favourable H-bond between *ba*NadE Tyr-33 and the adenine ring of NaAD would be lost in *ft*NadE, in which this residue is replaced by Ser. Finally, the side-chain orientation of the *ba*NadE His-258 residue, which is conserved in both enzymes, is dramatically different between the 2

BIOCHEMISTRY

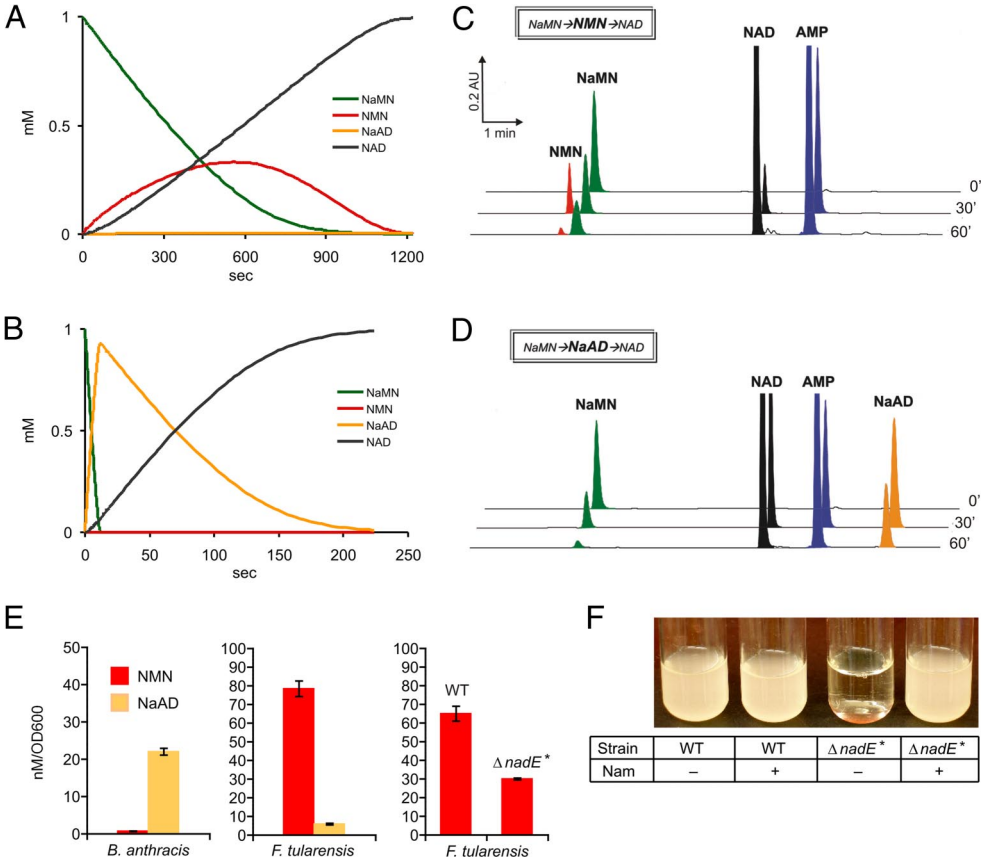


**Fig. 3.** Mathematical modeling, in vitro reconstitution, and in vivo assessment of the conventional (NaMN → NaAD → NAD, route I) and novel (NaMN → NMN → NAD, route II) pathways in *F. tularensis* and *B. anthracis*. (*A* and *B*) Examples of a simulated transient time-course of NaMN to NAD transformation for 2 binary mixtures: *ft*NadE*/*ft*NadM (*A*) and *ba*NadD/*ba*NadE (*B*). The details of model assumptions, boundary conditions, and additional results are provided in *SI Appendix*, *SI Text*. (*C* and *D*) In vitro reconstitution of a 2-step NaMN-to-NAD conversion by the same binary mixtures of pure recombinant enzymes: *ft*NadE*/*ft*NadM (*C*) and *ba*NadD/*ba*NadE (*D*), monitored by HPLC analysis at different time points. (*E*) HPLC-based assessment of the in vivo levels of NMN and NaAD intermediates: NaAD but not NMN is present in the crude extract from *B. anthracis* cells grown in rich media, whereas the extract of *F. tularensis* grown in rich media contains substantial amounts of NMN and a barely detectable level of NaAD. The NMN level is ≈2-fold higher in the wild-type strain compared with the *nadE** knockout mutant of *F. tularensis* (Δ*nadE**) grown in defined media (Chamberlain) supplemented with 200 μM nicotinamide. (*F*) The *ft*NadE* activity is required for the growth of *F. tularensis* in defined media in the absence of nicotinamide.

structures. In *ba*NadE this residue forms favorable stacking interactions with the NaAD adenine ring, whereas in the *ft*NadE structure it adopts a different rotamer conformation. The latter is stabilized by an H-bond with the main-chain carbonyl of Tyr-27 and by a stacking interaction with the Tyr-27 side-chain. Therefore, *ft*NadE* His-239 would clash with the adenosyl moiety of NaAD, while presenting no steric hindrance for binding of the NaMN substrate. One may notice that the structural differences observed in the substrate binding pocket of *ft*NadE* are relatively subtle. Nevertheless, altogether they lead to a substantial shift in the observed substrate preference of this enzyme, from dinucleotide (typical for other NadE enzymes) to mononucleotide, as reflected in an ≈30-fold difference in the apparent $K_m$ values (5.8 mM for NaAD compared with 0.2 mM for NaMN).

The structural basis of the substrate preference for NMN over NaMN displayed by *ft*NadM, the second enzyme of proposed route II of NAD synthesis (Fig. 1), is discussed in ref. 5. In Table 1, we provide the steady-state kinetic parameters of *ft*NadM, revealing an ≈400-fold discrimination of adenylylation of NMN vs. NaMN (based on the ratio of the apparent $k_{cat}/K_m$ values). A combination of the observed substrate preferences of both enzymes, *ft*NadE* and *ft*NadM, strongly suggests a preference for route II vs. route I for NAD synthesis in *F. tularensis*. For the comparison of this pathway with the conventional route I, we obtained the reciprocal kinetic parameters for *ba*NadE and *ba*NadD enzymes as described below.

**Enzymatic Characterization of *ba*NadE and *ba*NadD.** The 2 recombinant enzymes from *B. anthracis* were cloned with $His_6$-tag, expressed and purified as detailed in *SI Appendix*, *SI Text* and Fig. S3. The results of their steady-state kinetic analysis are shown in Table 1 and *SI Appendix*, Fig. S5. The NAD synthetase *ba*NadE displayed >3,000-fold preference for NaAD over NaMN, revealing not only an opposite substrate preference compared with *ft*NadE* but also a 50-fold stronger selectivity toward its preferred substrate. The steady-state kinetic parameters of *ba*NadD revealed even stronger substrate selectivity typical for NaMN adenylyltransferase of the NadD family. The observed preference for NaMN over NMN of *ba*NadD corresponds to an ≈100-fold increase in selectivity compared with the inverse preference of *ft*NadM. An extremely high substrate selectivity of both enzymes, *ba*NadE and *ba*NadD, indicated that NAD synthesis in *B. anthracis* would follow route I exclusively (without any appreciable contribution from route II). These results were used for mathematical modeling studies as described in the next section.

**Mathematical Modeling of NAD Biosynthetic Routes I and II.** The verified existence of NMN synthetase activity completes a symmetry of possible biochemical transformations generating NAD cofactor from the nearly universal NaMN precursor (Fig. 1). Whereas both reactions, adenylylation and amidation, are required to accomplish this transformation, the order of these 2 reactions (or, in general, the relative contribution of route I vs. route II) in any organism would depend on the relative catalytic efficiencies and substrate preferences of the respective enzymes. A general kinetic model of this system was developed and applied to simulate NaMN-to-NAD transformations for *F. tularensis* in comparison with *B. anthracis* (Fig. 3 *A* and *B*). The steady-state kinetic parameters identified for individual purified recombinant enzymes (Table 1) were used for the transient time-course and steady-state simulations in the 2 binary mixtures *ft*NadE*/*ft*NadM and *ba*NadD/*ba*NadE. Both types of simulations suggested that in *F. tularensis* the contribution of route II to the overall flux from NaMN to NAD in optimal conditions (defined by the ratio of the 2 enzymatic activities) may reach 100% (Fig. 3*A*). Although some contribution of route I and accumulation of the NaAD intermediate is possible in suboptimal conditions (e.g., if [*ft*NadE*] ≪ [*ft*NadM]), this situation is unlikely as it would lead to a very low overall flux through

the pathway. In the *B. anthracis* system, no contribution of route II and no appreciable accumulation of the off-pathway NMN intermediate are predicted by the simulations (Fig. 3*B*), even at a suboptimal ratio of the *ba*NadD/*ba*NadE enzymes. The more robust character of route I is a result of the more stringent substrate preferences of both *B. anthracis* enzymes compared with their counterparts from *F. tularensis*, as discussed above (Table 1). In addition to the important physiological implications, these simulations provided us with guidelines for the design of in vitro pathway reconstitution experiments (such as enzyme ratios and incubation times) aimed at the detection of pathway intermediates (see below).

**In Vitro Reconstitution of NAD Biosynthetic Routes I and II.** We used mixtures of purified recombinant enzymes *ft*NadE*/*ft*NadM and *ba*NadD/*ba*NadE for the in vitro reconstitution of respective pathways. A progression of NaMN-to-NAD conversion was initiated by adding the respective enzymes to the standard substrate mixture (1 mM NaMN, 2 mM ATP, and 4 mM $NH_4Cl$) and was monitored by HPLC analysis of aliquots taken at several time points (Fig. 3 *C* and *D*, and *SI Appendix*, Fig. S12). Both consecutive reactions are reversible, and both generate $PP_i$ as one of the products. To simplify the analysis and to make the reaction conditions similar to those used in mathematical simulations, we added inorganic pyrophosphatase to all reaction mixtures. This addition made both steps of either pathway technically irreversible, which indeed led to almost 100% conversion of NaMN to NAD accompanied by the generation of equimolar amounts of AMP. Despite this similarity, the key differences between the 2 systems were in the nature of the transient intermediates, NMN for the *ft*NadE*/*ft*NadM mixture vs. NaAD for the *ba*NadD/*ba*NadE mixture. Overall, the observed dynamics of substrate consumption and formation of the intermediate and final products were in line with mathematical simulations. This observation is supportive of both the generalized mathematical model and the assertion of alternative pathways in the compared species.

**In Vivo Assessment of NAD Biosynthesis in *B. anthracis* and *F. tularensis*.** To assess the physiological relevance of the proposed mechanism, we compared the NAD-related intermediates by HPLC in the extracts of *B. anthracis* and *F. tularensis* obtained in the log-phase of growth in rich media (*SI Appendix*, Fig. S13). A substantial level of NaAD intermediate was detected in *B. anthracis*, whereas the NMN level was below the detection threshold (Fig. 3*E*), in agreement with the model. In contrast, the level of NaAD intermediate was insignificant compared with NMN in *F. tularensis* (Fig. 3*E*). According to the steady-state simulations, some amounts of NaAD may accumulate in *F. tularensis* (generated by the residual NaMN adenylyltransferase activity of *ft*NadM) despite the negligible contribution of route I to the overall NAD biosynthetic flux. On the other hand, the NMN intermediate generated by *ft*NadE* within the major route II flux is not expected to accumulate in large quantities as it would be rapidly consumed by the *ft*NadM enzyme. However, the actual level of NMN in *F. tularensis* grown in the presence of nicotinamide could be somewhat higher because of the additional supply of NMN via *ft*NadV activity that was not accounted for by the described model (Fig. 1). Indeed, the observed level of NMN was >2-fold higher in the wild-type *F. tularensis* compared with the *nadE** mutant strain when both were grown in the defined media supplemented with 200 $\mu$M nicotinamide (Fig. 3*E*). This observation supports the proposed physiological activities of *ft*NadE* and *ft*NadV supports the fact that both enzymes actually contribute to NAD biosynthesis in *F. tularensis.* The in vivo NMN synthetase function of *ft*NadE* was additionally confirmed by the detection of the respective activity in the crude extract of the wild type but not in the *nadE** mutant of *F. tularensis* (*SI Appendix*, Fig. S14). The observation that the *nadE** mutant could grow normally in the presence but not in the absence of Nm (Fig. 3*F*) confirmed the existence of the *ft*NadE*-independent NadV-NadM route of Nm salvage (Fig. 1) in *F. tularensis.* The observed Nm auxotrophy of this mutant was fully suppressed by the introduction of the *ft*NadE*-coding gene on a plasmid. Overall, the observations listed above provided us with sufficient proof of the physiological relevance of the newly identified NMN synthetase activity of the *ft*NadE* enzyme. In contrast to the predicted and observed conditional essentiality of the *nadE** gene, the gene *nadM* encoding NMN adenylyltransferase should be essential under any growth conditions. This expectation is consistent with the biased distribution of the transposon insertions within the *nadM* gene that are present in all 3 viable *nadM* mutants from a transposon mutant library of *F. tularensis* subsp. *novicida* U112 (32). None of the mapped insertions would disrupt the N-terminal NMN adenylyltransferase domain, as in all 3 cases they occurred in the C-terminal ADPR pyrophosphatase domain, which is not involved in NAD biosynthesis and is expected to be fully dispensable.

## Discussion

A subsystems-based approach to genomic annotation and metabolic reconstruction allows us to efficiently expand our knowledge of biosynthetic pathways of key metabolites, such as vitamins and cofactors, across the rapidly growing collection of completely sequenced diverse genomes (9). This approach enables the accurate projection of the known genes and pathways from model organisms to others, cataloguing of pathway variants (33), and establishment of feasible metabolic scenarios (34). Among various implications of these efforts is the identification and critical assessment of drug targets for the development of new anti-infectives (8). The comparative genomic approach also allows us to reveal gaps (e.g., missing genes) and inconsistencies (e.g., genes out of context) in the existing knowledge and generate conjectures to reconcile the revealed problems (35).

This study provided the evidence of the existence of NMN synthetase enzymatic activity, and the first proof of functional heterogeneity within the NadE family. This prompted us to characterize the *ft*NadE* enzyme in detail, including the steady-state kinetics and 3D structural analysis. The key mechanistic and structural features of *ft*NadE*—such as ATP dependence, the ability to use $NH_3$ (but not Gln) as a N-source, the conservation of the dimeric structure, the overall fold, and many aspects of the active site topology—are quite similar to those of a typical single-domain bacterial NAD synthetase, such as *ba*NadE. However, the detailed structural comparison of these enzymes revealed several elements in the *ft*NadE* substrate-binding site that are likely responsible for its altered substrate preference. Among them are the residues likely contributing to the preferential binding of the mononucleotide (Q133, W233, R236) and a decreased affinity for the dinucleotide substrate (H233, Y27). Remarkably, the observed relatively subtle structural changes lead to a rather dramatic shift in substrate specificity: an ≈60-fold preference of NaMN over NaAD in *ft*NadE*, compared with an ≈3,000-fold inverse preference of NaAD over NaMN in *ba*NadE.

Of the 2 classes of biochemical transformations involved in the last steps of NAD biosynthesis (Fig. 1), variations in the substrate preference of respective enzymes have not been previously anticipated for the amidation step but are widely recognized for the adenylyltransferase reaction (36).

A combination of the observed substrate preference of both *F. tularensis* enzymes, *ft*NadE* for NaMN over NaAD and *ft*NadM for NMN over NaMN seem to be sufficient for reversing the usual order of biosynthetic steps toward the hypothesized route II (Fig. 1).

The difference between routes I and II was further analyzed using a generalized mathematical model of the 2-step NaMN-to-NAD conversion that accounts for all 4 possible reactions. The goal of the transient time-course simulations was to assess the reaction conditions for both pairs of enzymes, *ba*NadD/*ba*NadE and *ft*NadE*/*ft*NadM (enzyme concentrations and time points), that would allow us to detect the pathway intermediates. The simulations were simplified by forcing irreversibility of anabolic reactions by addition

of inorganic pyrophosphatase to all reaction mixtures used for the in vitro pathway reconstitution. In the nearly optimal conditions, the only intermediates that could be detected were NaAD for conventional route I and NMN for proposed route II (Fig. 3 *A–D*). The detection of the respective intermediates in the extracts from *B. anthracis* and *F. tularensis* (Fig. 3*E*) is consistent with the steady-state simulations, suggesting that the respective routes would provide the major contribution to the actual NAD biosynthetic flux in each of these organisms.

The genomic reconstruction of NAD biosynthesis in *F. tularensis* suggested that, in addition to the de novo pathway, this organism may generate NAD by conversion of Nam to NMN with nadV followed by NadM activity. This pathway bypasses the need of *ft*NadE*, which is consistent with the observed Nm auxotrophy of a viable *nadE** knockout mutant (Fig. 3*F*). The observed decrease of the overall NMN level (Fig. 3*E*) and the lack of any measurable NMN synthetase activity in this mutant (*SI Appendix*, Fig. S14) are consistent with the proposed physiological role of *ft*NadE*.

Comparative genomic reconstruction of NAD metabolism suggests that 2 other members of the same divergent branch of NadE family from *Mannhemimia succinoproducens* and *Actinobacillus succinogenes* may be additional species that harbor a version of route II (see *SI Appendix*, Table S1, Fig. S2 and *SI Text* for the details of this analysis and its evolutionary implications).

In summary, by combining a comparative genomic approach with in vitro and in vivo experiments we have established that the *nadE* gene of *F. tularensis* encodes an enzyme, NMN synthetase. The comparative analysis of the *ft*NadE* enzyme 3D structure revealed features contributing to its unusual substrate preference for NaMN over NaAD. This enzyme is involved in the first step of the alternative pathway, converting NaMN to NAD via the NMN intermediate. Although the *ft*NadE* enzyme is dispensable in *F. tularensis* because of the existence of the *ft*NadE*-independent salvage of Nm, the second enzyme of the pathway, NMN adenylyltransferase *ft*NadM, is absolutely required for NAD biogenesis. Therefore, the *ft*NadM enzyme likely constitutes a potential target for the development of therapies against this deadly pathogen.

## Methods

**Bioinformatic Tools.** A set of subsystems-based genomic annotations and metabolic reconstruction tools implemented in The SEED (9) were used to explore NAD metabolic machinery in bacteria (*SI Appendix*, Table S1 and Table S2). We used the PROMALS server (http://prodata.swmed.edu/promals/promals.php) to construct the multiple protein alignment (Fig. S7) and PHYLIP software version 3.62 to build the phylogenetic tree of representative members of the bacterial NadE family by the maximum-likelihood method (Fig. S8).

**Gene Cloning, Protein Overexpression, and Purification.** Proteins (*ft*NadM, *ft*NadE, *ba*NadD and *ba*NadE) were purified using standard protocols as described in *SI Appendix*, *SI Text*.

**Structural Analysis of *ft*NadE*.** Crystallographic analyses followed established methods as detailed in *SI Appendix* together with statistics (*SI Appendix*, Table S4), electron density map of the bound ligand (*SI Appendix*, Fig. S6*a*), and stereoview of catalytic site (*SI Appendix*, Fig. S6*b*).

**Enzyme Assays and Steady-State Kinetic Analysis.** Enzymatic characterization of purified proteins was performed using a series of specific assays, including continuous and discontinuous coupled enzyme assays and direct HPLC analysis, as described in detail in *SI Appendix*, *SI Text* together with initial rates plots (*SI Appendix*, Fig. S5).

**Mathematical Modeling.** Simulation of transient kinetics and steady-state fluxes of routes I and II for binary mixtures of *ft*NadE*/*ft*NadM and *ba*NadD/*ba*NadE enzymes were performed using Matlab as detailed in *SI Appendix*, *SI Text*.

**In Vivo Assessment of NAD Biosynthetic Intermediates.** Cellular levels of NMN and NaAD intermediates were determined by combining cellular extraction of pyridine nucleotides with enzymatic treatment as described in detail in *SI Appendix*, *SI Text*.

**ACKNOWLEDGMENTS.** We thank Xiaoqing Li for assistance in gene cloning; Dr. Y. Igarashi for help with sequence clustering; Ross Overbeek, Svetlana Gerdes, and other members of The SEED development team at the Fellowship for Interpretation of Genomes for the help with genome analysis; and David Scott for critical reading of the manuscript. This work was supported by National Institute of Allergy and Infectious Diseases Grant 5 R01 AI059146-02 (to A.L.O.) and National Institutes of Health Grant P01 AI57986 (to K.E.K.).

1. Begley TP, Kinsland C, Mehl RA, Osterman A, Dorrestein P (2001) The biosynthesis of nicotinamide adenine dinucleotides in bacteria. *Vitam Horm* 61:103–119.
2. Foster JW, Moat AG (1980) Nicotinamide adenine dinucleotide biosynthesis and pyridine nucleotide cycle metabolism in microbial systems. *Microbiol Rev* 44:83–105.
3. Magni G, Amici A, Emanuelli M, Raffaelli N, Ruggieri S (1999) Enzymology of NAD+ synthesis. *Adv Enzymol Relat Areas Mol Biol* 73:135–182.
4. Boshoff HI, *et al.* (2008) Biosynthesis and recycling of nicotinamide cofactors in mycobacterium tuberculosis. An essential role for NAD in nonreplicating bacilli. *J Biol Chem* 283:19329–19341.
5. Huang N, *et al.* (2008) Bifunctional NMN adenylyltransferase/ADP-ribose pyrophosphatase: Structure and function in bacterial NAD metabolism. *Structure* 16:196–209.
6. Gerdes SY, *et al.* (2002) From genetic footprinting to antimicrobial drug targets: Examples in cofactor biosynthetic pathways. *J Bacteriol* 184:4555–4572.
7. Jedrzejas MJ (2002) The structure and function of novel proteins of Bacillus anthracis and other spore-forming bacteria: Development of novel prophylactic and therapeutic agents. *Crit Rev Biochem Mol Biol* 37:339–373.
8. Osterman AL, Begley TP (2007) A subsystems-based approach to the identification of drug targets in bacterial pathogens. *Prog Drug Res* 131:133–170.
9. Overbeek R, *et al.* (2005) The subsystems approach to genome annotation and its use in the project to annotate 1000 genomes. *Nucleic Acids Res* 33:5691–5702.
10. Kurnasov OV, *et al.* (2002) Ribosylnicotinamide Kinase Domain of NadR Protein: Identification and Implications in NAD Biosynthesis. *J Bacteriol* 184:6906–6917.
11. Haferkamp I, *et al.* (2004) A candidate NAD+ transporter in an intracellular bacterial symbiont related to Chlamydiae. *Nature* 432:622–625.
12. McNeil LK, *et al.* (2007) The National Microbial Pathogen Database Resource (NMPDR): A genomics platform based on subsystem annotation. *Nucleic Acids Res* 35:D347–D353.
13. Larsson P, *et al.* (2005) The complete genome sequence of Francisella tularensis, the causative agent of tularemia. *Nat Genet* 37:153–159.
14. Gerdes S, *et al.* (2006) Essential genes on metabolic maps. *Curr Opin Biotechnol* 17:448–456.
15. Martin PR, Shea RJ, Mulks MH (2001) Identification of a plasmid-encoded gene from Haemophilus ducreyi which confers NAD independence. *J Bacteriol* 183:1168–1174.
16. Rongvaux A, *et al.* (2002) Pre-B-cell colony-enhancing factor, whose expression is up-regulated in activated lymphocytes, is a nicotinamide phosphoribosyltransferase, a cytosolic enzyme involved in NAD biosynthesis. *Eur J* Immunol 32:3225–3234.
17. Magni G, *et al.* (2004) Enzymology of NAD+ homeostasis in man. *Cell Mol Life Sci* 61:19–34.
18. Zhou T, *et al.* (2002) Structure of human nicotinamide/nicotinic acid mononucleotide adenylyltransferase. Basis for the dual substrate specificity and activation of the oncolytic agent tiazofurin. *J Biol Chem* 277:13148–13154.
19. Sorci L, *et al.* (2007) Initial-rate kinetics of human NMN-adenylyltransferases: Substrate and metal ion specificity, inhibition by products and multisubstrate analogues, and isozyme contributions to NAD+ biosynthesis. *Biochemistry* 46:4912–4922.
20. Yi CK, Dietrich LS (1972) Purification and properties of yeast nicotinamide adenine dinucleotide synthetase. *J Biol Chem* 247:4794–4802.
21. Wagner R, Wagner KG (1985) The pyridine-nucleotide cycle in tobacco Enzyme activities for the de-novo synthesis of NAD. *Planta V* 165:532–537.
22. Bieganowski P, Pace HC, Brenner C (2003) Eukaryotic NAD+ synthetase Qns1 contains an essential, obligate intramolecular thiol glutamine amidotransferase domain related to nitrilase. *J Biol Chem* 278:33049–33055.
23. Cantoni R, Branzoni M, Labo M, Rizzi M, Riccardi G (1998) The MTCY428.08 gene of Mycobacterium tuberculosis codes for NAD+ synthetase. *J Bacteriol* 180:3218–3221.
24. Hara N, *et al.* (2003) Molecular identification of human glutamine- and ammonia-dependent NAD synthetases. Carbon-nitrogen hydrolase domain confers glutamine dependency. *J Biol Chem* 278:10914–10921.
25. Hughes KT, Ladika D, Roth JR, Olivera BM (1983) An indispensable gene for NAD biosynthesis in Salmonella typhimurium. *J Bacteriol* 155:213–221.
26. Nessi C, Albertini AM, Speranza ML, Galizzi A (1995) The outB gene of Bacillus subtilis codes for NAD synthetase. *J Biol Chem* 270:6181–6185.
27. Willison JC, Tissot G (1994) The Escherichia coli efg gene and the Rhodobacter capsulatus adgA gene code for NH3-dependent NAD synthetase. *J Bacteriol* 176:3400–3402.
28. McDonald HM, *et al.* (2007) Structural adaptation of an interacting non-native C-terminal helical extension revealed in the crystal structure of NAD+ synthetase from Bacillus anthracis. *Acta Crystallogr D* 63:891–905.
29. Zalkin H (1993) The amidotransferases. *Adv Enzymol Relat Areas Mol Biol* 66:203–309.
30. Zalkin H (1985) NAD synthetase. *Methods Enzymol* 113:297–302.
31. Rizzi M, *et al.* (1996) Crystal structure of NH3-dependent NAD+ synthetase from Bacillus subtilis. *EMBO J* 15:5125–5134.
32. Gallagher LA, *et al.* (2007) A comprehensive transposon mutant library of Francisella novicida, a bioweapon surrogate. *Proc Natl Acad Sci USA* 104:1009–1014.
33. Ye Y, Osterman A, Overbeek R, Godzik A (2005) Automatic detection of subsystem/pathway variants in genome analysis. *Bioinformatics* 21:478–486.
34. DeJongh M, *et al.* (2007) Toward the automated generation of genome-scale metabolic networks in the SEED. *BMC Bioinformatics* 8:139.
35. Osterman A, Overbeek R (2003) Missing genes in metabolic pathways: A comparative genomics approach. *Curr Opin Chem Biol* 7:238–251.
36. Magni G, *et al.* (2004) Structure and function of nicotinamide mononucleotide adenylyltransferase. *Curr Med Chem* 11:873–885.